An integral boundary layer engineering model for vortex generators implemented in XFOIL

De Tavernier, Delphine; Baldacchino, Daniel; Ferreira, Carlos

DOI
10.1002/we.2204

Publication date
2018

Document Version
Final published version

Published in
Wind Energy

Received: 15 November 2017 | Revised: 16 March 2018 | Accepted: 3 April 2018
DOI: 10.1002/we.2204

WILEY

RESEARCH ARTICLE

An integral boundary layer engineering model for vortex generators implemented in XFOIL

Delphine De Tavernier | **Daniel Baldacchino** | **Carlos Ferreira**

Wind Energy Section, Faculty of Aerospace Engineering, Delft University of Technology, Kluyverweg 1, 2629HS Delft, The Netherlands

Correspondence
Delphine De Tavernier, Wind Energy Section, Faculty of Aerospace Engineering, Delft University of Technology, Kluyverweg 1, 2629HS Delft, The Netherlands.
Email: d.a.m.detavernier@tudelft.nl

Funding information
EU's FP7 AVATAR, Grant/Award Number: FP7-ENERGY-2013-1/no. 608396; Dutch TKI Wind op Zee D4REL, Grant/Award Number: TKIW02007

Abstract

To assess and optimize vortex generators (VGs) for flow separation control, the effect of these devices should be modelled in a cost and time efficient way. Therefore, it is of interest to extend integral boundary layer models to analyse the effect of VGs on airfoil performance. In this work, the turbulent boundary layer formulation is modified using a source term approach. An additional term is added to the shear-lag equation, to account for the increased dissipation due to streamwise vortex action in the boundary layer, forcing transition at the VG leading edge where applicable. The source term is calibrated and a semi-empirical relation is set up and implemented in XFOIL. The modified code is capable of addressing the effect of the VG height, length, inflow angle, and chordwise position on the airfoil's aerodynamic properties. The predicted polars for airfoils with VGs show a good agreement with reference data, and the code robustness is demonstrated by assessing different airfoil families at a wide range of Reynolds numbers.

KEYWORDS

integral boundary layer, separation control, source term, vortex generator, Xfoil

1 | INTRODUCTION

For the next generation of wind turbines, manufacturers aim to design multimegawatt rotors to improve the competitiveness of wind energy technology. To up-scale wind turbines, novel technologies are required and new design challenges will appear. One such aerodynamic challenge is the management of separated flow. Preventing or at least delaying separation over the blades can positively affect the annual energy production (AEP). On top of that, the magnitude and severe variations of the aerodynamic loads associated with separating flows can be reduced, mitigating structural fatigue issues. In the wind energy industry, separation control is often realized by using passive vortex generators (VGs).

Vortex generators improve the resistance of a boundary layer against flow separation by re-energizing the flow close to the surface. The streamwise vortices shed from the free tips of the VGs enhance mixing between the high-energy flow in the outer part of the boundary layer with the low-energy regions near the walls (see Schubauer and Spangenberg.[1]) The physics involved is nontrivial and poses a number of modelling challenges. To achieve a cost-effective scale up of current turbines, it will become necessary to evolve towards a multidisciplinary design process where VGs are already incorporated early in the design phase. To assess and optimize the use of VGs, there will be a need to effectively model these devices in a cost and time efficient manner.

1.1 | Background

Numerous VG modelling techniques have been explored in literature, most of which use computational fluid dynamics (CFD). The most direct and intuitive approach is to model the effect of VGs by including them as a local geometrical protrusion in the domain. This approach requires a fully

Nomenclature: c, Airfoil chord (m); C_d, Drag coefficient (-); C_D, Dissipation coefficient (-); C_f, Friction coefficient (-); C_l, Lift coefficient (-); C_τ, Shear stress coefficient (-); h_{VG}, Vortex generator height (m); h^*_{VG}, Vortex generator height, normalized with c (-); H, Boundary layer shape factor (-); I_{ST}, Source term integral (-); l_{VG}, Vortex generator length (m); l^*_{VG}, Vortex generator length, normalized with c (-); S_{VG}, Source term (-); U_∞, Freestream velocity (m/s); U_{VG}, Velocity at VG, normalized with U_∞ (-); U_e, Boundary layer edge velocity, normalized with U_∞ (-); x, Streamwise coordinate (m); x_{tr}, Laminar-turbulent transition location (m); x_{VG}, Vortex generator location (m); α, Angle of attack (°); β_{VG}, Vortex generator inflow angle (°); δ, Boundary layer thickness (m); δ^*, Displacement thickness (m); θ, Momentum thickness (m); λ, Source term decay rate (-); σ_0, Source term strength (-)

3-dimensional treatment and a dense grid due to the complexity of the flow and the small size of the VGs (see Nikolaou and Politis,[2] Jirasek,[3] and von Stillfried et al[4]).

In 1999, Bender et al[5] developed a simplified technique in which the effect of VGs was modelled without including the geometry explicitly in the computational mesh. This approach is now commonly known as the BAY model. The method relies on the addition of a side force as a source term in the momentum equation. This essentially introduces and simulates swirl in the flow, giving rise to the formation of vortices produced by the VGs. Jirasek[3,6] suggested further improvements to the original model by refining the definition of the source term. Besides adding a source term based on a lateral lift force, other researchers constructed source terms based on a predetermined vortex circulation, or on the velocity induced by this circulation according to the Biot-Savart law. This method is referred to as a vortex-source model. Research based on this method is found in the spanwise averaged CFD method of Nikolaou and Politis[2] and the 3-dimensional approach by Zhang.[7] As Jirasek[3] noted, the key problem of these kind of models is that the initial circulation introduced by the VG needs to be known beforehand. Later, Tornblom and Johansson[8] presented a method in which a Reynolds stress approach is used in a statistical sense. They explicitly introduced the vortex-added velocity and associated stresses into the differential Reynolds stress transport equations to mimic the increased mixing due to the VGs. [8,9]

Despite considerable advances with CFD-based methods, such techniques are generally more time and resource consuming, compared with the industry workhorses that are integral boundary layer (IBL) tools and blade element momentum methods. This makes them impractical for use in iterative design processes. Therefore, it is of interest to extend integral boundary layer models to analyse the effect of flow mixing devices on airfoil performance. Limited research is done in such a modelling approach incorporating VGs, and it is useful to consider the physics involved from an integral boundary layer perspective. Drela[10] argues that VGs promote increased dissipation by introducing streamwise vortices into the boundary layer, which consequently increases the sustainable adverse pressure gradient. Lengani et al[11] demonstrated this by analysing the dissipation mechanisms in a separating duct controlled by vane-type vortex generators. Dissipation in this sense refers to the drain of mean flow kinetic energy through the action of the shear stress with the mean strain rate, essentially, through enhanced mixing.

In essence, these observations are captured in the IBL method proposed by Michael Kerho and Brian Kramer.[12] In their approach, the VG-added mixing effect was incorporated into the XFOIL code through an enhancement of the turbulence production in the turbulent boundary layer formulation by modifying the stress transport formulation. The authors suggested modifying the boundary layer dissipation through the shear stress coefficient by introducing a stepwise increase in the production term, which decreases exponentially downstream. An obvious limitation of this approach is that the fully 3-dimensional flow field induced by an array of vortex generators is represented and modelled by a 2-dimensional integral boundary layer formulation. However, it is possible for 2D design codes to handle these complex situations and offer a global or spanwise-averaged effect of VGs for design direction.

1.2 | Research objective

Kerho and Kramer's[12] source term approach was proposed for a specific case with a single row of co-rotating VGs. Their focus was on natural-laminar-flow airfoils at relatively low operational Reynolds numbers with VGs installed far downstream for trailing edge separation control. Therefore, the objective of this article is to model the effect of VGs in an IBL code (ie, XFOIL) by extending the source term implementation and overall code robustness for thicker airfoils over a wider operational envelope. This objective will be approached by the following:

1. Modifying the closure relations using a source term approach.
2. Setting up a relation between the source term, VG geometry, and boundary layer properties, using CFD and experimental airfoil reference data.
3. Verifying and validating the implementation and assessing the code robustness.

The article proceeds in Section 2 with a description of the methodology, modelling rationale, and boundary layer modifications in the context of vortex generators. Validation results are presented in Section 3 through comparisons with flat plate experiments and airfoil measurements. Further discussion is presented in Section 4 and concluding remarks in Section 5.

2 | APPROACH AND METHODS

2.1 | Integral boundary layer code

The integral boundary layer code XFOIL is a viscous-inviscid interaction method designed for predicting airfoil flows and performance.[13] In this framework, the flow is decomposed into 2 regions: the inviscid outer flow where viscosity can be neglected and the thin, viscous shear layer, that is, the inner flow, where the boundary layer plays an important role.

The outer flow is solved using a linear-vorticity streamfunction panel method. A 2-dimensional inviscid airfoil flowfield is composed of a free stream flow, a vortex sheet of strength γ on the airfoil surface, and a source sheet of strength σ on the airfoil surface and in the trailing wake.[13] The system is closed with the Kutta condition applied at the trailing edge.

The viscous boundary layer solution is obtained using the so-called numerical integral method. The partial differential equations for continuity, momentum and energy can be reworked and transformed into the familiar ordinary differential equations in terms of integral quantities:

$$\frac{\tau_w}{\rho U_e^2} = \frac{C_f}{2} = \frac{d\theta}{dx} + (2+H)\frac{\theta}{U_e}\frac{dU_e}{dx}, \tag{1}$$

$$\frac{2D}{\rho U_e^3} = 2C_D = \frac{d\theta^\star}{dx} + \left(3 + \frac{2H^{\star\star}}{H^\star}\right)\frac{\theta^\star}{U_e}\frac{dU_e}{\partial x}. \tag{2}$$

This method therefore determines the integral thickness and key shear quantities, namely, displacement thickness $\delta^\star$, momentum thickness θ, friction coefficient C_f, and the dissipation coefficient C_D. [10] The integral momentum and kinetic energy equations are consequently combined with a chain of laminar and turbulent closure relations in order to make the problem determinate.[14] Finally, both solutions are coupled using a fully simultaneous coupling scheme described by Drela et al.[15] The entire nonlinear equation set is solved simultaneously as a fully coupled system using a global Newton-Raphson method.

2.2 | Boundary layer formulation modification

The effect of VGs can be introduced in a number of ways. In this case, the boundary layer formulation is modified through the dissipation term. To do so, a source term approach is used, in which an additional production term is added to the turbulence closure relations. The choice of closure relation should be physically consistent, but also facilitate implementation, without compromising the code convergence behaviour. Thus, 2 sub-goals were to determine (1) in which equation to incorporate the source term and (2) to explore the behaviour of this source term over the streamwise domain.

2.2.1 | Source term implementation

The source term is implemented into the rate equation (or shear-lag equation), an ordinary differential equation for the shear stress level inside the boundary layer. The equation models turbulence history effects that dominate turbulence intensity (see Drela and Giles[16]) Additionally, the rate equation depends on an empirical constant K_c, controlling the reactivity of the boundary layer, and on the equilibrium shear stress coefficient $C_{\tau_{EQ}}$. The latter represents the shear stress level that would exist if the local boundary layer would be in equilibrium, in this sense, meaning that the boundary layer profile for a turbulent flow exhibits a behaviour analogous to the similar flows of laminar boundary layers.[17] In slowly changing flows, the flow is almost in equilibrium and thus C_τ closely follows $C_{\tau_{EQ}}$. However, this does not hold for rapidly changing flows, and thus, the rate equation plays an important role in modelling the lag effect. A case in point are vortical flows, in which the Reynolds stresses are known to lag the mean strain field.[18]

A simple expression for $C_{\tau_{EQ}}$ can be obtained from the well-known G-β locus of equilibrium boundary layers proposed by Clauser.[16] The source term implementation is presented in Equation 3 where S_{VG} represents the source term itself:

$$\frac{\delta}{C_\tau}\frac{dC_\tau}{dx} = K_c\left(\left(C_{\tau_{EQ}}^{1/2} + S_{VG}\right) - C_\tau^{1/2}\right). \tag{3}$$

Because $C_{\tau_{EQ}}$ is seen as the fundamental parameter of the rate equation, the VG source term is added explicitly to the equilibrium shear stress coefficient $C_{\tau_{EQ}}$, effectively enhancing the production term of the turbulent kinetic energy budget. In this sense, the non-equilibrium nature of VG flow increases the tendency of the boundary layer to depart from its equilibrium state.

This implementation was also favourable considering the convergence speed and numerical stability of XFOIL. Qualitatively speaking, these modifications promote an increased momentum thickness but reduce the displacement thickness. The shape factor decreases and the skin friction coefficient will increase.[10,11] It is important to note that these trends may be skewed by the physical presence of the devices, which according to Schubauer and Spangenberg,[1] cause local jumps in δ^* and θ that are amplified with the developing boundary layer. This will become evident in the following section.

2.2.2 | Source term shape function

The source term shape function is selected so as to mimic the streamwise vortex strength decay from mixing devices (see, eg, Lögdberg et al[19] and Baldacchino et al[20]). Such studies have shown that vortex strength decay is roughly exponential and arises because of the presence of wall shear, boundary layer turbulence and mutual interference between adjacent vortices. On the other hand, vortices shed by VGs do not appear abruptly, and generally require around one vane chord length to develop before reaching their full rolled-up intensity. Therefore, the selected source term shape is given by Equation 4 where the source term develops gradually before decaying exponentially.

As shown in Figure 1, the shape function differs from the expression used by Kerho and Kramer,[12] who proposed instead a simple step function. The new source term expression consists of 3 variables: the source term strength σ_0, decay rate λ, and the location of the VG with respect to the

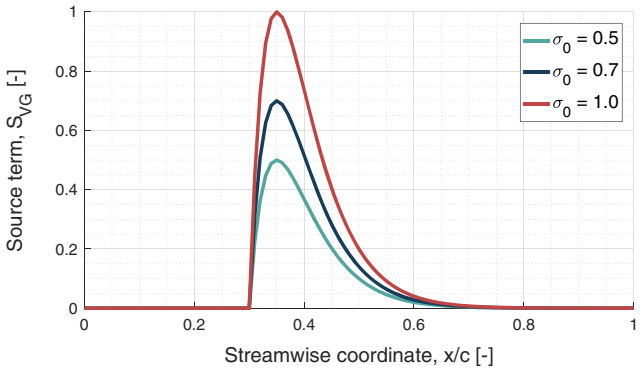

FIGURE 1 Source term variation with respect to chordwise position for 3 different source term strengths σ_0 and a constant decay rate λ of 20.0 [Colour figure can be viewed at wileyonlinelibrary.com]

leading edge. Assuming that the source term is related to the strength of the shed circulation, it is expected that the source term strength σ_0 and decay rate λ will be a function of the VG configuration and the local boundary layer properties.

$$S_{VG} = \sigma_0 \cdot \left(\frac{x - x_{VG}}{c}\right) \cdot \exp\left(-\lambda\left(\frac{x - x_{VG}}{c}\right)\right). \tag{4}$$

2.3 | Laminar-turbulent transition

XFOIL uses the e^N method for predicting natural transition.[21] This method assumes that transition occurs when the most unstable Tollmien-Schlichting wave in the boundary layer has grown by a given factor e^N, where $N = 9$ for natural transition.[13]

Vortex generators that are typically sized on the order of the boundary layer thickness will likely lead to bypass-type transition within a short region. Research has shown that small VGs can actually delay transition, by attenuating critical perturbations in the boundary layer.[22] However, this is out of scope of the applications envisaged in this work. A simplified transition definition is used that assumes that VGs promote flow transition at their leading edge, independent of their configuration:

$$x_{tr} = x_{tr,free} \qquad \text{if } x_{tr,free} < x_{VG}, \tag{5}$$

$$x_{tr} = x_{VG} \qquad \text{if } x_{tr,free} > x_{VG}, \tag{6}$$

where x_{tr} represents the transition location with respect to the airfoil leading edge. The validity of this assumption will depend somewhat on the VG configuration and the local pressure gradient. However, in many practical applications, VGs are mounted on a strip that itself can enforce transition, as illustrated in Figure 2.

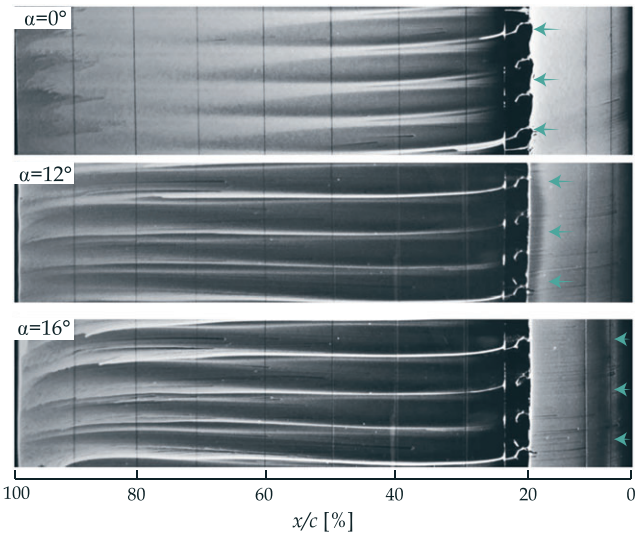

FIGURE 2 Oil-flow visualizations of the DU97W300 airfoil depicting the (suction side) advance of the transition region ahead of the VG array with angle of attack (images obtained from the campaign described in Baldacchino et al[24]) [Colour figure can be viewed at wileyonlinelibrary.com]

2.4 | Source term calibration

Of the 3 source term shape function variables, the source strength σ_0 and the decay rate λ are unknown and expected to depend on the airfoil/VG configuration. The required value of both parameters is determined here based on a calibration process using reference data obtained from high-fidelity numerical simulations and measurements. Data sets are adopted from studies of Timmer and van Rooij,[23] Baldacchino et al,[20,24] Manolesos and Voutsinas,[25] and the public database provided by the AVATAR project.[26-28] These cover a variety of VG configurations, airfoil families, and inflow conditions. A summary of the data sets is given in the Appendix. For different VG configurations in various flow conditions, the source term is determined in 3 steps:

1. Analyse the effect of the source term parameters on lift and drag.
2. Define the target aerodynamic properties.
3. Determine the required source term parameters.

This procedure is summarized in Figure 3. Throughout the remainder of this article, cases without and with vortex generators are referred to as the *clean case* and *VG case*.

2.4.1 | Part 1—source term effect

The effect of different source terms with different strength and decay parameters is presented in Figure 4 for 2 different angles of attack. Increasing the source term strength and decay at low angles of attack (ie, below stall) results in a decreasing lift coefficient and increasing drag. However, at low angles, the sensitivity is small because the boundary layer is less receptive to the added dissipation. At high angles of attack, the opposite is true and the increased mixing gradually takes effect with increasing angle of attack.

One may ascertain that multiple combinations of source term strength and decay predict the same lift and drag coefficient. It has been established that all these combinations of strength σ_0 and decay λ constants share the same value of the source term integral, as shown in Figure 5. This source term integral I_{ST}, is the area enclosed by the source term function:

$$I_{ST} = \int_0^1 S_{VG}\, d(x/c). \tag{7}$$

The integral is numerically determined based on the airfoil panelling using the trapezoidal rule. In keeping with the IBL modelling ethos, the definition of I_{ST} reduces the number of unknowns (originally the strength σ_0 and decay λ) to a single variable.

2.4.2 | Part 2—target lift polar

To account for the discrepancies of the clean polar predicted by the airfoil code, corrected (target) polars expected to be found by the airfoil code are introduced. With reference to Steps 1 and 2 in Figure 3, the lift slope discrepancy between clean XFOIL predictions and reference data is first calculated. The slopes were evaluated in the interval $\alpha = [0^\circ, 4^\circ]$. Finally, in Step 3, the slope correction factor is applied to the reference lift polar for the VG case. This procedure avoids the source term accounting for inherent inaccuracies of the integral boundary layer code. The corrected lift polar is referred to as the target lift curve and is thus thought to be a more representative reference with which to calibrate the empirical function.

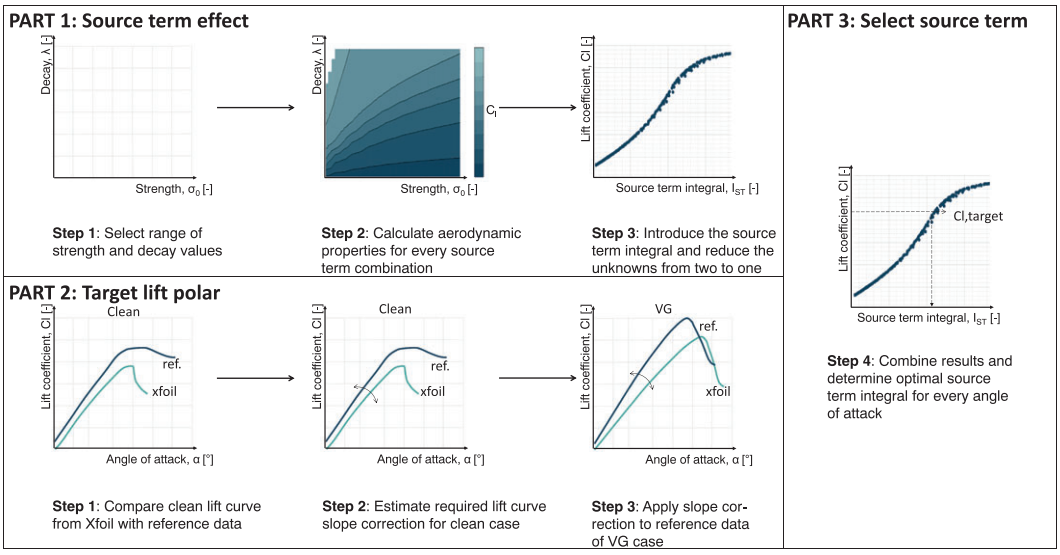

FIGURE 3 Overview of the source term calibration process [Colour figure can be viewed at wileyonlinelibrary.com]

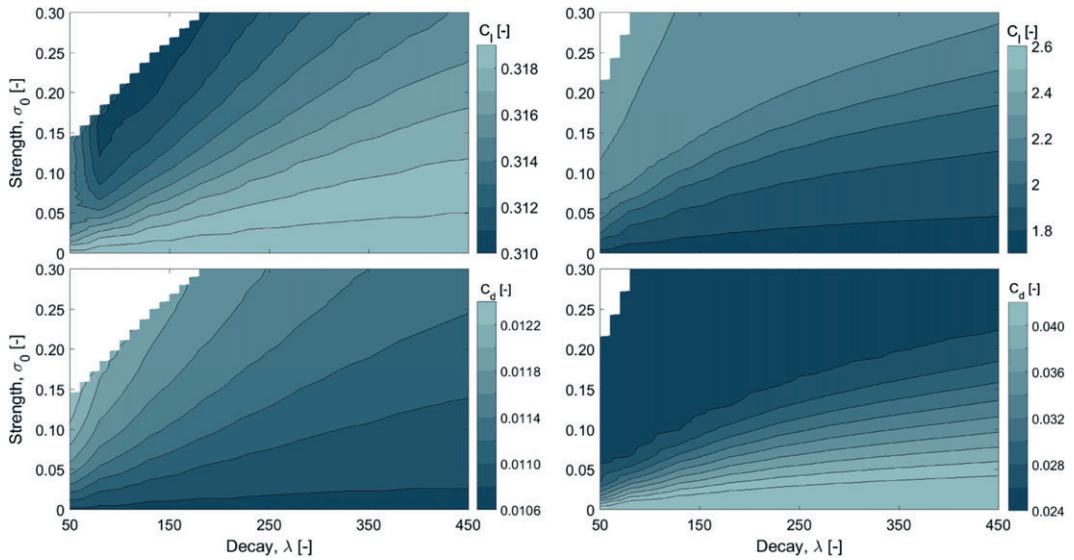

FIGURE 4 Effect of the source term strength and decay on the lift and drag of the DU97W300 airfoil ($Re = 2 \times 10^6$) [Colour figure can be viewed at wileyonlinelibrary.com]

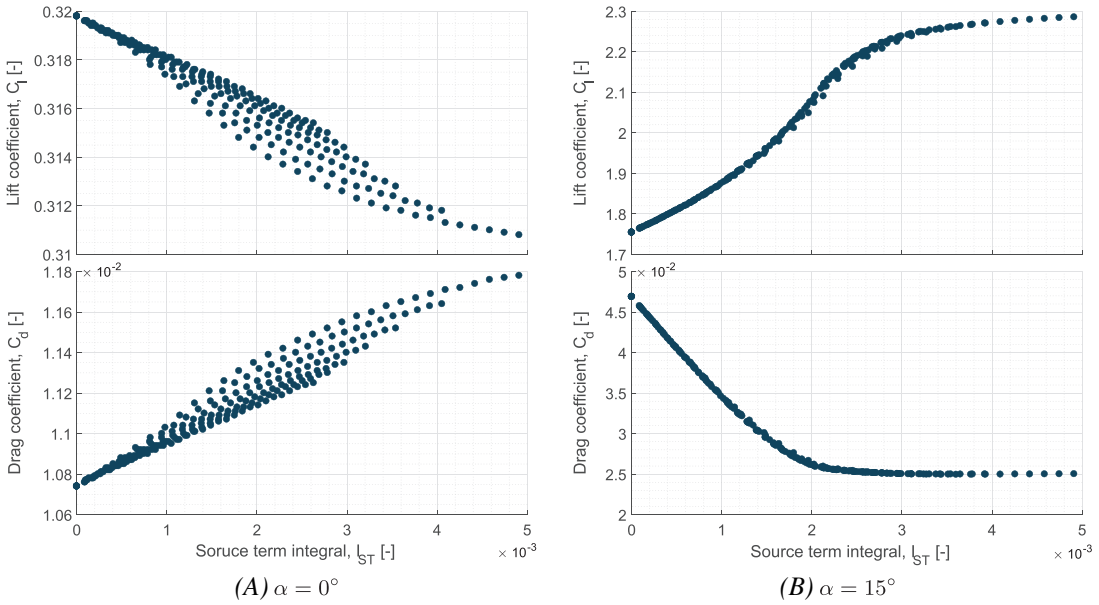

FIGURE 5 Effect of the source term integral on lift and drag of the DU97W300 airfoil (Re = 2x10^6) [Colour figure can be viewed at wileyonlinelibrary.com]

2.4.3 | Part 3—source term selection

The determination of the optimal source term is based primarily on the lift coefficient. The drag coefficient is not found suitable because integral boundary layer codes significantly underestimate drag in clean case and because the source term approach does not account for the additional profile drag of the VG itself. Boundary layer measurements with vortex generators providing reliable integral properties are sparsely available and thus also unsuitable for the present purpose.

2.5 | Source term semi-empirical relation

To relate the source term magnitude to airfoil/VG parameters, a semi-empirical relation is set up. The source term magnitude should depend on the effectiveness of the VG, defined here as the strength of the shed vortex. The independent variables are subsequently selected following thin airfoil theory. Accordingly, the amount of circulation generated by a flat plate in ideal conditions depends on the chord length, the angle of attack, and the incoming flow velocity. Analogously, here we consider (1) the VG length l_{VG}, (2) the angle between the VG chord line and the incoming flow β_{VG}, (3) the flow velocity at the VG tip, U_{VG}, and (4) the VG height, h_{VG}/l_{VG}, scaled as the vane aspect ratio. These variables, schematically presented in Figure 6, have been previously identified as being directly correlated to the strength of the shed vortex (see Wendt and Reichert,[29] Angele and

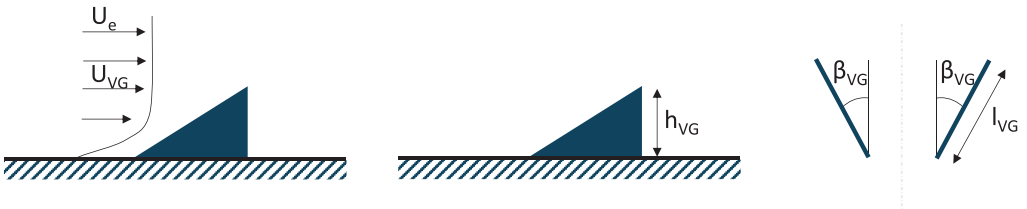

FIGURE 6 Schematic representation of the flow velocity at the vortex generator (VG) tip, the VG height, length, and inflow angle [Colour figure can be viewed at wileyonlinelibrary.com]

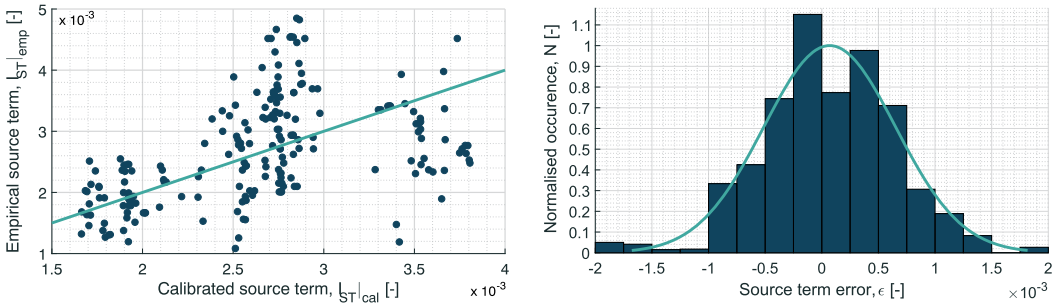

FIGURE 7 Assessment of residuals from the linear regression procedure [Colour figure can be viewed at wileyonlinelibrary.com]

Muhummad-Klingmann,[30] and Ashill et al[31]).

Equation 8 is used as a basis for setting up the semi-empirical relation. Using a weighted least-squares regression of the calibrated source terms, $C_0, C_1, \cdots, C_3$ are determined. The reliability of such a calibration depends of course on the quality of the predictions in clean conditions. To account for this, the calibration procedure uses a weighting function taking into account the error in predicting the lift slope, maximum lift coefficient, and stall angle compared with the reference data. Additionally, focus is placed on higher angles of attack since at lower angles, the effect of the source term on lift and drag is smaller than the expected accuracy of the code. This process is also shown in Figure 3.

$$I_{ST} = C_0 \cdot \left(\frac{h^\star_{VG}}{l^\star_{VG}} \right)^{C_1} \cdot (l^\star_{VG} \cdot \sin \beta_{VG})^{C_2} \cdot (U_{VG})^{C_3}, \tag{8}$$

where $C_0 = 0.0240, C_1 = 0.2754, C_2 = 0.4507, C_3 = 0.2987$.

The VG parameters $h^\star_{VG}$ and $l^\star_{VG}$ represent the non-dimensional vortex generator height and length with respect to the airfoil chord. To retrieve the flow velocity at the VG tip (U_{VG}), the Swafford boundary layer velocity profile as used in XFOIL is reconstructed using the momentum thickness Reynolds number Re_θ, the kinematic shape parameter H, the edge velocity U_e, and the boundary layer thickness δ. [13,32] Figure 7 provides the error distribution between the calibrated source term, $S_{VG}|_{cal}$ and the empirical fit, $S_{VG}|_{emp}$. The residuals are approximately normally distributed.

The source term expression (Equation (8)) is implemented in XFOIL in such a way as to minimize the required user interaction. Therefore, the only inputs required are the VG geometry: the VG height, length, inflow angle, and position with respect to the airfoil leading edge. The inflow velocity U_{VG} is calculated internally using an iterative process that is consequently used to update the value of the source term according to the empirical relation.

3 | RESULTS

The VG modelling capabilities are assessed in this section. Results are presented for a canonical case of a flat plate with and without vortex generators and subsequently for 3 airfoil sets controlled using vortex generators. The former allows a more straightforward assessment of integral boundary layer properties, whereas the latter provides basis for global comparison.

3.1 | Boundary layer properties

The control effect of a vortex generator is indirectly assessed by analysis of the IBL properties. Baldacchino et al[20] acquired measurements for a 6 m-long flat-plate turbulent boundary layer in the presence of vortex generators. The boundary layer was tripped at 2.5% from the leading edge of the flat plate and the baseflow pressure distribution was approximately constant. The vortex generators used in this case were of rectangular planform with $h^\star_{VG} = 8.3 \times 10^{-4}$, $l^\star_{VG} = 2.5 \times 10^{-3}$, $\beta_{VG} = 18°$, and $x_{VG}/c = 0.164$. The flat plate geometry, consisting of a leading-edge region, a flat (uniform) centre piece, and a trailing edge was defined and panelled in XFOIL. The nose portion (the leading 1% chord) was modelled using a Hermite

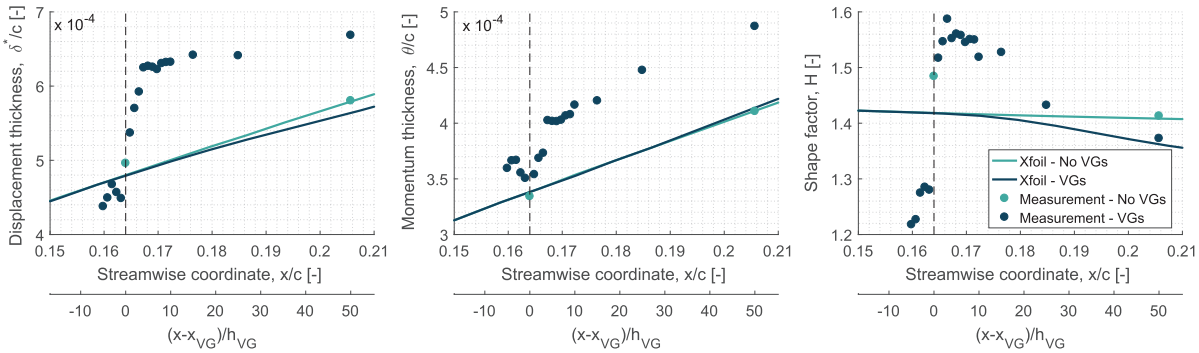

FIGURE 8 Comparison of measured (symbols) and predicted (lines) integral boundary layer properties [Colour figure can be viewed at wileyonlinelibrary.com]

polynomial that was merged with the middle section using a square root blending function. The trailing 20% chord was modelled as the aft 70% of a NACA0010 symmetric airfoil (further details of this method are found in Sanders.[33]) A uniform pressure distribution was obtained at $\alpha = 0°$.

The predicted evolution of the boundary layer properties is shown in Figure 8 for the clean and VG case. The relatively short range of the measurements downstream limits the extent of the comparisons. However, the measured and predicted trends compare reasonably well. Notable discrepancies exist at the location of the VG itself: the measurements demonstrate somewhat of a step increase in δ^* and θ. The vortex action gradually enhances the boundary layer state, seen as an eventual decrease in the shape factor (Figure 8C). However, a passive device is itself a source of drag that manifests as a mass and momentum deficit in the developing boundary layer, over and above the effect of the developing vortex. Schubauer and Spangenberg[1] originally demonstrated this aft of passive devices in a boundary layer wind tunnel. They observed that the evolution of the relative momentum deficit remained rather constant. This implies that the device drag could potentially be modelled as a stepwise perturbation that would subsequently be convected and modulated with the developing boundary layer. Since the present model implementation does not account for this penalty drag, this additional deficit cannot be captured.

3.2 | Global performance assessment

This part of the validation aims to (1) validate the source term expression and (2) demonstrate the code robustness. This will be achieved by validating the source term sensitivity with VG location, height, and inflow angle by comparison with data sets outside the reference database.

3.2.1 | Source term expression

In Figure 9A and 9B, reference polars and XFOIL calculations for various VG positions are presented. The reference data were obtained by Baldacchino et al[24] on a DU97W300 airfoil model with 0.65-m chord at a Reynolds number of 2×10^6 in free transition. The model was equipped with counter-rotating Delta-shaped VGs with a height of 10 mm and length of $3h_{VG}$, set under an inflow angle of 15°. Vortex generators were positioned at 30%, 40%, and 50% chord. Results show that placing the VGs further upstream increases maximum lift and postpones the stalling angle. At low angles of attack, the closer the VGs are to the leading edge, the higher the drag. Within the current modelling framework, this occurs primarily because of the earlier forced transition to turbulence, minimizing the lower-drag laminar flow region over the airfoil. These observations are evident in the experimental data, which are reasonably well predicted by XFOIL.

Figure 10 shows a similar comparison using the same reference data set, comparing the effect of the VG height. The Delta-shaped VGs are located at 40% chord from the airfoil leading edge and have a height of 5 and 10 mm, all other parameters dictated through geometric similarity. Increasing the VG height at this location improves their effectiveness in separation delay but also introduces more drag at pre-stall angles of attack.

The effect of the inflow angle is presented in Figure 11. The reference data originates from a numerical parametric study performed within the AVATAR project.[27] The synthetic data were generated using fully turbulent, geometry-resolving CFD computations on a 33% thick FFAW3333 airfoil with a chord length of 5.84 m. The use of synthetic data permitted a comparison for a high Reynolds number (in this case 14×10^6) for which experimental data with VGs is not readily available. The airfoil was equipped with 30-mm high and 90-mm long counter-rotating Delta-shaped VGs, mounted at 40% chord. Evidently, increasing the vane inflow angle from 15° to 25° increases the maximum lift. The drag at low angles of attack increases for higher vane angles and decreases at high angles of attack as separation is delayed. Note that while the drag increases at a similar rate after maximum lift is attained, the numerical computations predict an earlier merging point than XFOIL. This is the angle at which the VGs, in all cases considered, are rendered completely ineffective because of large scale separation, resulting in a collapse of all polars.

3.2.2 | Code robustness

Additional comparisons are made with the measurements reported in Fouatih et al.[34] These authors present an experimental parametric study on different VG geometrical parameters for optimizing flow separation control of a NACA4415 airfoil. The experiments were carried out in a subsonic wind tunnel at a Reynolds number of 2×10^5 in free transition.

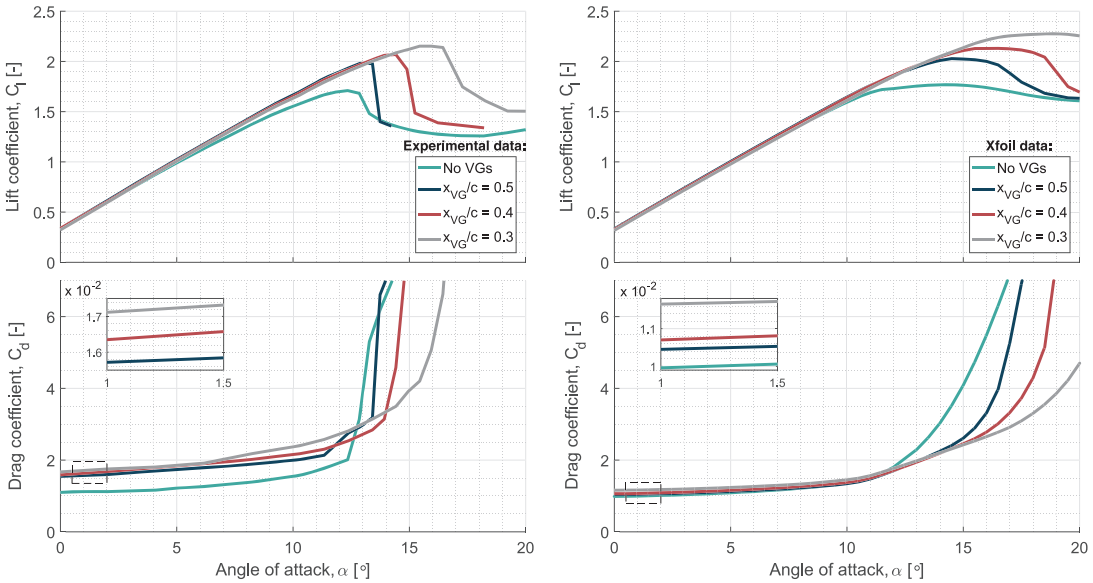

(A) Experimental data *(B) XFOIL data*

FIGURE 9 Effect of the vortex generator (VG) location on the lift and drag polar for a DU97W300 airfoil at $Re = 2 \times 10^6$ [Colour figure can be viewed at wileyonlinelibrary.com]

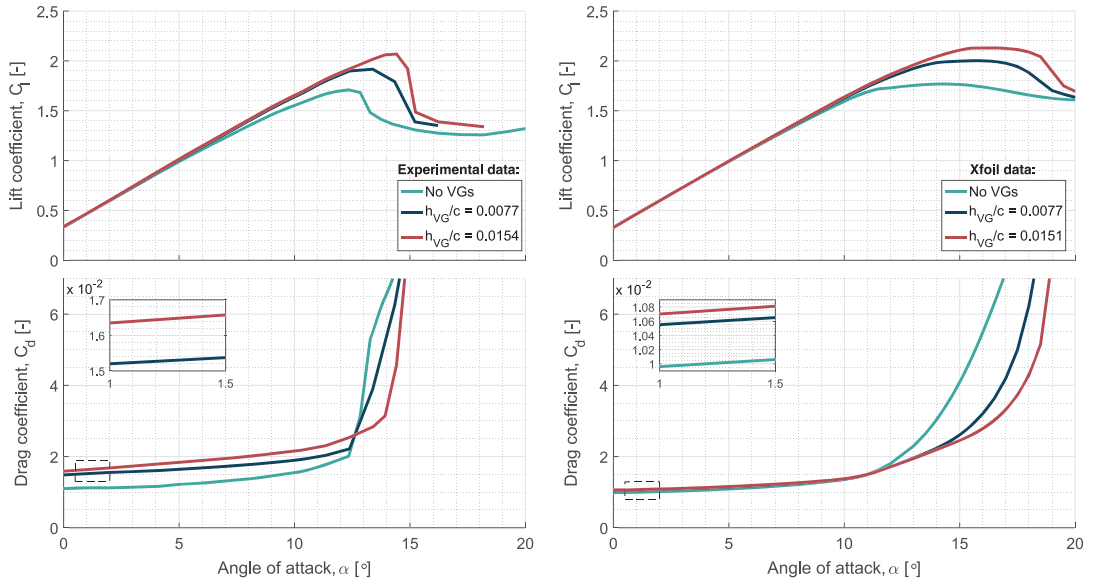

(A) Experimental data *(B) XFOIL data*

FIGURE 10 Effect of the vortex generator (VG) height on the lift and drag polar for a DU97W300 airfoil at $Re = 2 \times 10^6$ [Colour figure can be viewed at wileyonlinelibrary.com]

Figure 12A to 12C presents the sensitivity of the relative change in maximum lift ($\Delta C_{l,max}$) to the VG height h_{VG}/c, VG location x_{VG}/c, and the inflow angle β_{VG}. Except for the VG location, the trends are generally captured well, along with the order of magnitude.

4 | DISCUSSION

4.1 | Source term expression

The regression coefficients of the expression (Equation (8)) reveal that the source term integral increases with increasing VG length, VG height, inflow angle, and flow velocity. The capability of the airfoil code to model VGs significantly depends on the quality of the source term expression. This in turn is limited by the quality of the calibration database, and how well represented the key variables are in those data sets. These limitations can be summarized as follows:

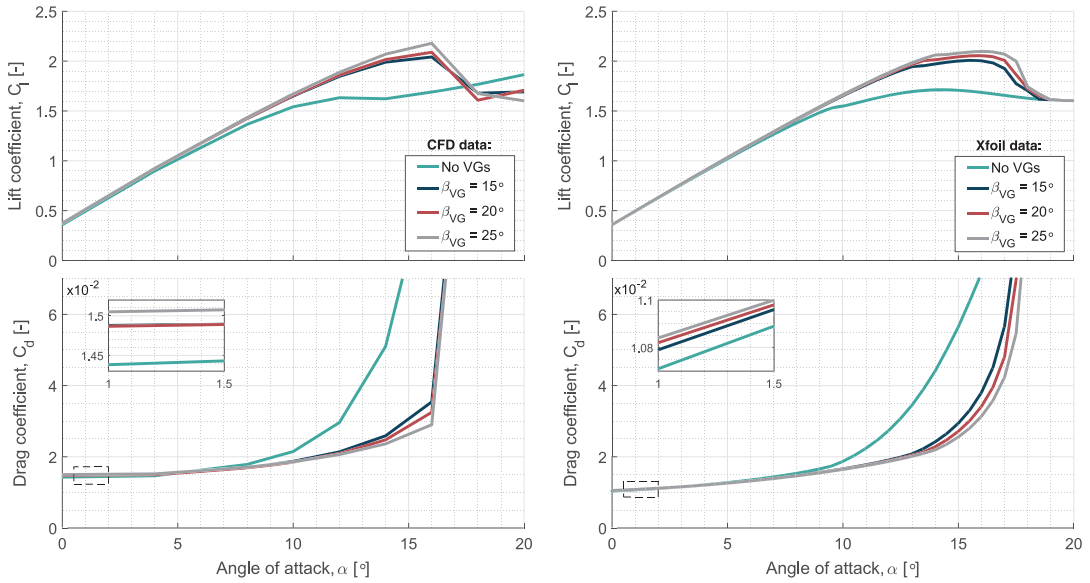

(A) CFD data *(B) XFOIL data*

FIGURE 11 Effect of varying the vortex generator (VG) inflow angle on the lift and drag polar for an FFAW3333 airfoil at $Re = 14 \times 10^6$ [Colour figure can be viewed at wileyonlinelibrary.com]

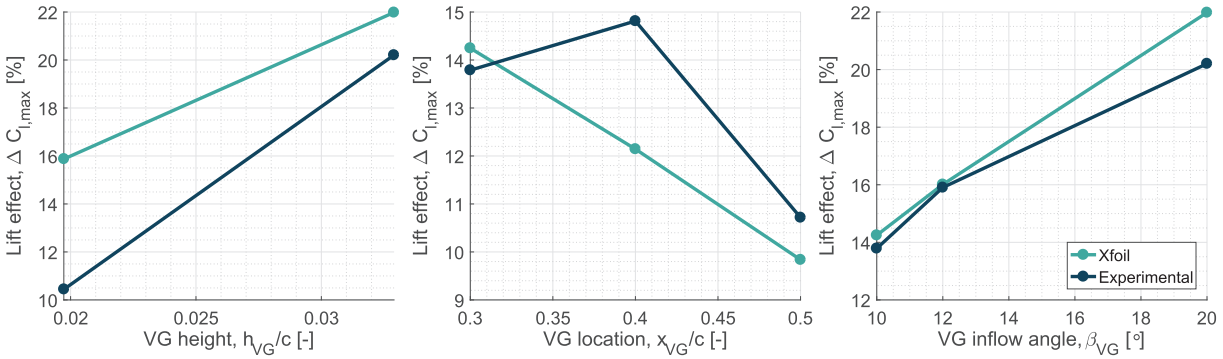

(A) VG height *(B) VG location* *(C) VG inflow angle*

FIGURE 12 Effect of varying vortex generator (VG) parameters on the maximum lift coefficient for a NACA4415 airfoil at $Re = 2 \times 10^5$ [Colour figure can be viewed at wileyonlinelibrary.com]

- **Error uncontrolled airfoil:** For the uncontrolled performance (without VGs), XFOIL mostly overestimates the lift slope as well as the maximum lift coefficient and underestimates the drag. Despite efforts to anticipate for this using correct target polars, the calibrated source term will to some extent also account for the discrepancies in uncontrolled airfoil predictions.
- **Reference data:** The performance of the code is limited by the availability, consistency, and quality of the reference data. Not all VG parameters (eg, pair spacing and VG shape) were sufficiently represented in the database. Improving this representation is seen as a potential continuous improvement of the presented method.
- **Boundary layer properties:** The velocity at the VG is calculated using the edge velocity, integral boundary layer properties, and expressions for the boundary layer thickness and velocity profile. This includes additional uncertainties and affects the quality of the source term expression.

4.2 | Validation

Comparing all available reference cases with the XFOIL predictions, we can establish goodness measures, as shown in Figure 13A to13C. These show the error distribution for the maximum lift coefficient, the stall angle, and the drag coefficient at zero angle of attack. The error is defined as the difference between the reference and predicted XFOIL values, normalized with respect to the reference value. The following observations can be made:

- **Maximum lift coefficient:** The error for the maximum lift coefficient is normally distributed with a mean value near zero. This result was expected since the composition of the source term expression was based on the maximum lift coefficient. With a 90% confidence interval, the error of the predicted maximum lift coefficient with respect to the reference value will be within ±12%.

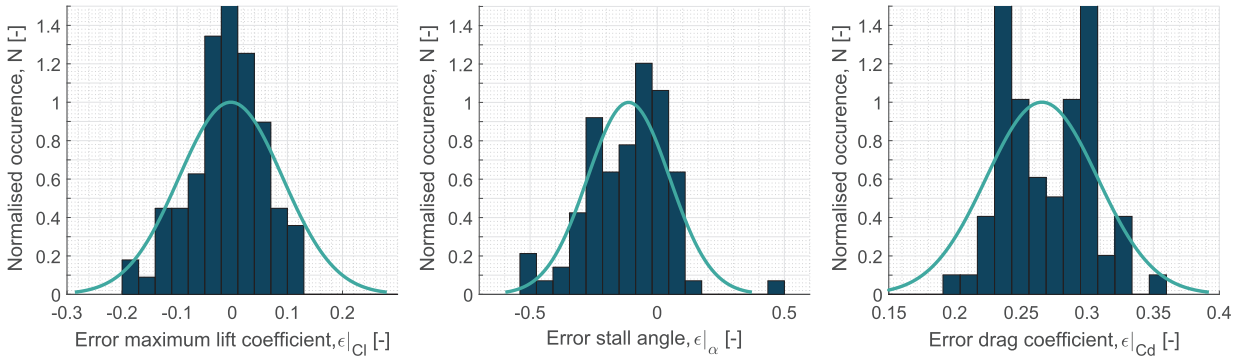

(A) Lift coefficient *(B) Stall angle* *(C) Drag coefficient ($\alpha = 0^\circ$)*

FIGURE 13 Error distribution between the reference data and the XFOIL calculations [Colour figure can be viewed at wileyonlinelibrary.com]

- **Stall angle:** While the modal value is roughly zero centred, the mean error is approximately −10%, meaning that XFOIL mostly overpredicts the stall angle. However, this is a tendency of the present code for predictions even without VGs.
- **Drag coefficient:** The drag coefficient is consistently underpredicted. The drag at zero angle of attack found by XFOIL is more than 25% lower than the reference value. The net increment in drag by adding VGs is lower than given by the reference data since the parasitic VG drag has not been accounted for in the present model.

The methodology presented demonstrates a potentially useful engineering approach for modelling vortex generators in integral boundary layer codes. Reasonable predictions have been demonstrated. Some of the limitations and assumptions discussed prior can be better managed with the following suggestions:

1. **Reference data:** An expanded reference database to improve the representation of important variables within the calibration process.
2. **VG profile drag:** The model currently does not account for the additional drag introduced by the VGs. One possibility is to introduce a deficit term in the momentum equation correlated to the device geometry. Additionally, the closure relations deployed by XFOIL such as that for skin friction have been traditionally obtained for 2D naturally developing boundary layers. Studying the influence of vortex-induced perturbations on such closure relations can improve code robustness.
3. **Laminar-turbulent transition:** Transition criteria based on the critical Reynolds number can be implemented, which determines whether the VGs are capable of promoting bypass type transition.
4. **2D vs 3D:** The fully 3-dimensional flow field induced by an array of VGs is represented and modelled by a 2-dimensional integral boundary layer formulation. In the close proximity of the VG, the shed vortices create a fully 3-dimensional flow field. The modified XFOIL code is validated to model the global effect on lift and drag of airfoils equipped with VGs, meaning the spanwise averaged behaviour of the periodic behaviour of an array. Validating the physical correctness of this assumption could allow for better physical modelling of the VG effect.

5 | CONCLUSION

This article demonstrates a method for modelling the effect of VGs using the integral boundary layer code XFOIL. The methodology builds on the source term approach introduced by Kerho and Kramer[12]. This was realized by adding an additional term to the equilibrium shear stress coefficient of the shear-lag equation, accounting for the increased dissipation due to streamwise vortex action in the boundary layer. A gradual step input followed by exponential decay was introduced at the VG location, mimicking the inception and evolution of an embedded streamwise vortex. This perturbation was described using 3 variables: the source term strength, the decay rate, and the location of the VGs.

Synthesizing these parameters, the source term integral was defined and correlated with the VG geometry and inflow conditions. This was set up using a least-square regression to calibrate the expression parameters with an extensive reference database. The resulting expression gives the required value of the source term integral as a function of the VG height, length, inflow angle, and flow velocity at the tip of the VG.

The modified XFOIL code can predict the aerodynamic behaviour of an airfoil equipped with VGs. The new code is capable of addressing the effect of the VG height, length, inflow angle, and chordwise position but is not expected to capture subtle differences in VG geometry. The error on the maximum lift coefficient is normally distributed with a mean value near zero. The stall angle is mostly overpredicted, but this is in line with the clean airfoil predictions. The drag at zero angle of attack found by XFOIL is more than 25% lower than the reference value, which can be explained because of the lack in modelling the parasitic drag of the VGs itself.

Overall, the predicted polars for airfoils with VGs showed a good agreement with the reference data and the code is demonstrated to be robust and able to model different airfoil families at a wide range of Reynolds numbers. The source term approach is proven to be promising and can be elaborated further considering some of the suggested improvements.

6 | SOFTWARE AVAILABILITY

Source code and executables of the newly developed XFOIL tool for vortex generators may be publicly accessed at https://github.com/ddetavernier/XFOILVG.

ACKNOWLEDGEMENTS

The work has been partially funded by the EU's FP7 AVATAR project under the grant FP7-ENERGY-2013-1/no. 608396 and the Dutch TKI Wind op Zee D4REL project, grant number TKIW02007.

ORCID

Delphine De Tavernier http://orcid.org/0000-0002-8678-8198
Daniel Baldacchino http://orcid.org/0000-0002-4515-237X

REFERENCES

1. Schubauer GB, Spangenberg WG. Forced mixing in boundary layers. *J Fluid Mech*. 1959;8(1):10-32.
2. Nikolaou IG, Politis ES. Modelling the flow around airfoils equipped with vortex generators using a modified 2D Navier-Stokes solver. *J Sol Energy Eng*. 2005;127(2):223-233.
3. Jirasek A. Vortex generator model and its application to flow control. *J Aircr*. 2005;42(6):1486-1491.
4. von Stillfried F, Wallin S, Johansson AV. Evaluation of a vortex generator model in adverse pressure gradient boundary layers. *Am Inst Aeronaut Astronaut*. 2011;49(5):982-993.
5. Bender EE, Anderson BH, Yagle PJ. Vortex generator modelling for Navier-Stokes codes. In: 3rd Jt. ASME/JSME Fluids Eng Conf. ;1999; San Francisco, CA. 1-7. ISBN 0791819612. https://doi.org.FEDSM99-6919.
6. Jirasek A. A modified vortex generator model and its application to complex aerodynamic flows. *Swed Def Res Agency, Div Aeronaut*. 2004.
7. Lei Z, Ke Y, JianZhong X, MingMing Z. Modeling of delta-wing type vortex generators. *Sci China Technol Sci*. 2011;54(2):277-285.
8. Tornblom O, Johansson AV. A Reynolds stress closure description of separation control with vortex generators in a plane asymmetric diffuser. *AIP Phys Fluids*. 2007;19(11):115108.
9. von Stillfried F. Computational fluid-dynamics investigations of vortex generators for flow-separation control. *PhD Thesis*: KTH Royal Institute of Technology; 2012.
10. Drela M. *Flight Vehicle Aerodynamics*. Cambridge, Massachusetts: The MIT Press; 2014. Chapter 4.
11. Lengani D, Simoni D, Ubaldi M, Zunino P, Bertini F. Turbulent boundary layer separation control and loss evaluation of low profile vortex generators. *Exp Thermal Fluid Sci*. 2011;35:1505-1513.
12. Kerho M, Kramer B. Enhanced airfoil design incorporating boundary layer mixing devices. In: 41st Aerospace Sciences Meeting and Exhibit, Aerospace Sciences Meetings. 2003;AIAA-2003-0211.
13. Drela M. *Xfoil: An Analysis and Design System for Low Reynolds Number Airfoils*. Berlin: Springer; 1989. In Low Reynolds Number Aerodynamics.
14. Van Garrel A. Integral boundary layer methods for wind turbine aerodynamics. *ECN*. 2003;ECN-C–04-004.
15. Drela M, Giles MB, Thompkins WT. Newton solution of coupled Euler and boundary layer equations. In: Presented at the Third Symposium on Numerical and Physical Aspects of Aerodynamic Flows; 1985; New York. 143-154.
16. Drela M, Giles MB. Viscous-inviscid analysis of transonic and low Reynolds number airfoils. *Am Inst Aeronaut Astronaut*. 1986;25(10):1347-1355.
17. Libby PA. *An Introduction to Turbulence*. New York: Taylor and Francis; 1996.
18. Chow JS, Zilliac GG, Bradshaw P. Mean and turbulence measurements in the near field of a wingtip vortex. *AIAA J*. 1997;35(10):1561-1567.
19. Lögdberg O, Fransson JHM, Alfredsson PH. Streamwise evolution of longitudinal vortices in a turbulent boundary layer. *J Fluid Mech*. 2009;623(27):27-58.
20. Baldacchino D, Ragni D, Ferreira CS, van Bussel GJ. Towards integral boundary layer modelling of vane-type vortex generators. In: 45th AIAA Fluid Dynamics Conference. American Institute of Aeronautics and Astronautics; 2015:AIAA-2015-3345.
21. van Ingen JL. A suggested semi-empirical method for the calculation of the boundary layer transition region. Technical Report VTH-74, The Netherlands, Delft University of Technology, Dept. of Aerospace Engineering; 1956.
22. Shahinfar S, Sattarzadeh SS, Fransson JHM, Talamelli A. Revival of classical vortex generators now for transition delay. *Phys Rev Lett*. 2012;109(7):074501.
23. Timmer W, van Rooij R. Summary of the Delft University wind turbine dedicated airfoils. *Am Soc Mech Eng*. 2003;125:488-496.
24. Baldacchino D, Ferreira C, De Tavernier D, Timmer WA, van Bussel GJW. Experimental parameter study for passive vortex generators on a 30% thick airfoil. *Wind Energy (In press)*. 2018. https://doi.org/10.1002/we.2191.
25. Manolesos M, Voutsinas SG. Experimental investigation of the flow past passive vortex generators on an airfoil experiencing three-dimensional separation. *J Wind Eng Ind Aerodyn*. 2015;142:130-148.
26. Baldacchino D, Manolesos M, Ferreira C, et al. Experimental benchmark and code validation for airfoils equipped with passive vortex generators. *J Phys Conf Ser*. 2016;753(2). https://doi.org/10.1088/1742-6596/753/2/022002.
27. Manolesos M, Prospathopoulos J. CFD & experimental database of flow devices. AVATAR Task 3.1,; February 2015.
28. Ferreira C, Salcedo AG, Baldacchino D, Aparicio M. Development of aerodynamic codes for modelling of flow devices on aerofoils and rotors. AVATAR Task 3.2; November 2015.

29. Wendt BJ, Reichert BA. The modelling of symmetric airfoil vortex generators. In: 34th Aerospace Sciences Meeting and Exhibit. American Institute of Aeronautics and Astronautics; 1996.
30. Angele KP, Muhummad-Klingmann B. The effect of streamwise vortices on the turbulence structure of a separating boundary layer. *Eur J Mech*. 2005;24:539-554.
31. Ashill P, Fulker L, Hackett K. Research at DERA on sub-boundary layer vortex generators (SBVGs). In: American Institute of Aeronautics and Astronautics; 2001. 39th Aerospace Sciences Meeting and Exhibit.
32. Swafford TW. Analytical approximation of two-dimensional separated turbulent boundary-layer velocity profiles. *AIAA J*. 1983;21(6):923-926.
33. Sanders M. The Boundary layer over a flat plate. http://essay.utwente.nl/65492/; 2014.
34. Fouatih O, Medale M, Imine O, Imine B. Design optimization of the aerodynamic passive flow control on NACA 4415 airfoil using vortex generators. *Eur J Mech B Fluids*. 2015;56:82-96.

How to cite this article: De Tavernier D, Baldacchino D, Ferreira C. An integral boundary layer engineering model for vortex generators implemented in Xfoil. *Wind Energy*. 2018;1-16. https://doi.org/10.1002/we.2204

APPENDIX: DATA SETS FOR CALIBRATION

TABLE A1 Overview of the experimental and computational database

No.	Airfoil Model		VG Configuration								Flow Properties	
	Airfoil	Chord Length, m	Shape	Rotation	Height, mm	Length, mm	Internal Distance, mm	External Distance, mm	Inflow Angle [°]	Position [x/c]	Reynolds Number [-]	Transition
LTT01	DU97W300	0.65	Delta	Counter	5	15	17.5	35	15	0.1	2.0×10^6	Free
LTT02	DU97W300	0.65	Delta	Counter	5	15	17.5	35	15	0.2	2.0×10^6	Free
LTT03	DU97W300	0.65	Delta	Counter	5	15	17.5	35	15	0.3	2.0×10^6	Free
LTT04	DU97W300	0.65	Delta	Counter	5	15	17.5	35	15	0.4	2.0×10^6	Free
LTT05	DU97W300	0.65	Delta	Counter	5	15	17.5	35	15	0.5	2.0×10^6	Free
LTT06	DU97W300	0.65	Delta	Counter	10	30	35	70	15	0.2	2.0×10^6	Free
LTT07	DU97W300	0.65	Delta	Counter	10	30	35	70	15	0.3	2.0×10^6	Free
LTT08	DU97W300	0.65	Delta	Counter	10	30	35	70	15	0.4	2.0×10^6	Free
LTT09	DU97W300	0.65	Delta	Counter	10	30	35	70	15	0.5	2.0×10^6	Free
LTT10	DU97W300	0.65	Delta	Counter	5	15	17.5	35	15	0.2	1.0×10^6	Free
LTT11	DU97W300	0.65	Delta	Counter	5	15	17.5	35	15	0.4	1.0×10^6	Free
LTT12	DU97W300	0.65	Delta	Counter	10	30	35	70	15	0.2	1.0×10^6	Free
LTT13	DU97W300	0.65	Delta	Counter	10	30	35	70	15	0.4	1.0×10^6	Free
LTT14	DU97W300	0.65	Delta	Counter	5	15	17.5	35	15	0.2	3.0×10^6	Free
LTT15	DU97W300	0.65	Delta	Counter	5	15	17.5	50	15	0.2	2.0×10^6	Free
LTT16	DU97W300	0.65	Delta	Counter	5	15	17.5	35	12	0.2	2.0×10^6	Free
LTT17	DU97W300	0.65	Delta	Counter	5	15	17.5	35	18	0.2	2.0×10^6	Free
LTT18	DU97W300	0.65	Delta	Counter	5	15	17.5	35	15	0.1	2.0×10^6	Forced
LTT19	DU97W300	0.65	Delta	Counter	5	15	17.5	35	15	0.2	2.0×10^6	Forced
LTT20	DU97W300	0.65	Delta	Counter	5	15	17.5	35	15	0.3	2.0×10^6	Forced
LTT21	DU97W300	0.65	Delta	Counter	5	15	17.5	35	15	0.4	2.0×10^6	Forced
LTT22	DU97W300	0.65	Delta	Counter	5	15	17.5	35	15	0.5	2.0×10^6	Forced
LTT23	DU97W300	0.65	Delta	Counter	10	30	35	70	15	0.2	2.0×10^6	Forced
LTT24	DU97W300	0.65	Delta	Counter	10	30	35	70	15	0.3	2.0×10^6	Forced
LTT25	DU97W300	0.65	Delta	Counter	10	30	35	70	15	0.4	2.0×10^6	Forced
LTT26	DU97W300	0.65	Delta	Counter	10	30	35	70	15	0.5	2.0×10^6	Forced
AVA01	DU331	6.06	Delta	Counter	10	30	20	50	20	0.25	1.6×10^7	Forced
AVA02	DU331	6.06	Delta	Counter	12	36	24	60	20	0.25	1.6×10^7	Forced
AVA03	DU331	6.06	Delta	Counter	15	45	30	75	20	0.25	1.6×10^7	Forced
AVA04	DU331	6.06	Delta	Counter	18	54	36	90	20	0.25	1.6×10^7	Forced
AVA05	DU331	6.06	Delta	Counter	30	90	60	150	20	0.25	1.6×10^7	Forced
AVA06	DU331	6.06	Delta	Counter	36	108	72	180	20	0.25	1.6×10^7	Forced
AVA07	DU331	6.06	Delta	Counter	60	180	120	300	20	0.25	1.6×10^7	Forced

TABLE A1 (Continued)

No.	Airfoil Model		VG Configuration						Flow Properties			
	Airfoil	Chord Length, m	Shape	Rotation	Height, mm	Length, mm	Internal Distance, mm	External Distance, mm	Inflow Angle [°]	Position [x/c]	Reynolds Number [-]	Transition
AVA08	DU331	6.06	Delta	Counter	15	45	30	75	20	0.3	1.6×10^7	Forced
AVA09	DU331	6.06	Delta	Counter	18	54	36	90	20	0.3	1.6×10^7	Forced
AVA10	DU331	6.06	Delta	Counter	30	90	60	150	20	0.3	1.6×10^7	Forced
AVA11	DU331	6.06	Delta	Counter	36	108	72	180	20	0.3	1.6×10^7	Forced
AVA12	DU331	6.06	Delta	Counter	60	180	120	300	20	0.3	1.6×10^7	Forced
AVA13	DU331	6.06	Delta	Counter	15	45	30	75	20	0.4	1.6×10^7	Forced
AVA14	DU331	6.06	Delta	Counter	18	54	36	90	20	0.4	1.6×10^7	Forced
AVA15	DU331	6.06	Delta	Counter	30	90	60	150	20	0.4	1.6×10^7	Forced
AVA16	DU331	6.06	Delta	Counter	36	108	72	180	20	0.4	1.6×10^7	Forced
AVA17	DU331	6.06	Delta	Counter	60	180	120	300	20	0.4	1.6×10^7	Forced
AVA18	DU331	6.06	Delta	Counter	90	270	180	450	20	0.4	1.6×10^7	Forced
AVA19	FFAW3333	5.84	Delta	Counter	10	30	20	50	20	0.25	1.4×10^7	Forced
AVA20	FFAW3333	5.84	Delta	Counter	12	36	24	60	20	0.25	1.4×10^7	Forced
AVA21	FFAW3333	5.84	Delta	Counter	15	45	30	75	20	0.25	1.4×10^7	Forced
AVA22	FFAW3333	5.84	Delta	Counter	18	54	36	90	20	0.25	1.4×10^7	Forced
AVA23	FFAW3333	5.84	Delta	Counter	30	90	60	150	20	0.25	1.4×10^7	Forced
AVA24	FFAW3333	5.84	Delta	Counter	36	108	72	180	20	0.25	1.4×10^7	Forced
AVA25	FFAW3333	5.84	Delta	Counter	60	180	120	300	20	0.25	1.4×10^7	Forced
AVA26	FFAW3333	5.84	Delta	Counter	15	45	30	75	20	0.3	1.4×10^7	Forced
AVA27	FFAW3333	5.84	Delta	Counter	18	54	36	90	20	0.3	1.4×10^7	Forced
AVA28	FFAW3333	5.84	Delta	Counter	30	90	60	150	20	0.3	1.4×10^7	Forced
AVA29	FFAW3333	5.84	Delta	Counter	36	108	72	180	20	0.3	1.4×10^7	Forced
AVA30	FFAW3333	5.84	Delta	Counter	60	180	120	300	20	0.3	1.4×10^7	Forced
AVA31	FFAW3333	5.84	Delta	Counter	15	45	30	75	20	0.4	1.4×10^7	Forced
AVA32	FFAW3333	5.84	Delta	Counter	18	54	36	90	20	0.4	1.4×10^7	Forced
AVA33	FFAW3333	5.84	Delta	Counter	30	90	60	150	20	0.4	1.4×10^7	Forced
AVA34	FFAW3333	5.84	Delta	Counter	36	108	72	180	20	0.4	1.4×10^7	Forced
AVA35	FFAW3333	5.84	Delta	Counter	60	180	120	300	20	0.4	1.4×10^7	Forced
AVA36	FFAW3333	5.84	Delta	Counter	90	270	180	450	20	0.4	1.4×10^7	Forced
AVA37	FFAW3333	5.84	Delta	Counter	10	30	20	50	15	0.4	1.4×10^7	Forced
AVA38	FFAW3333	5.84	Delta	Counter	10	20	20	50	20	0.4	1.4×10^7	Forced
AVA39	FFAW3333	5.84	Delta	Counter	10	30	15	50	20	0.4	1.4×10^7	Forced

TABLE A1 (Continued)

No.	Airfoil Model		VG Configuration								Flow Properties	
	Airfoil	Chord Length, m	Shape	Rotation	Height, mm	Length, mm	Internal Distance, mm	External Distance, mm	Inflow Angle [°]	Position [x/c]	Reynolds Number [-]	Transition
AVA40	FFAW3333	5.84	Delta	Counter	10	30	20	45	20	0.4	1.4×10^7	Forced
AVA41	FFAW3333	5.84	Delta	Counter	10	30	20	55	20	0.4	1.4×10^7	Forced
AVA42	FFAW3333	5.84	Delta	Counter	10	30	25	50	20	0.4	1.4×10^7	Forced
AVA43	FFAW3333	5.84	Delta	Counter	10	30	20	50	25	0.4	1.4×10^7	Forced
AVA44	DU331	6.06	Delta	Counter	10	30	20	50	15	0.4	1.6×10^7	Forced
AVA45	DU331	6.06	Delta	Counter	10	20	20	50	20	0.4	1.6×10^7	Forced
AVA46	DU331	6.06	Delta	Counter	10	30	15	50	20	0.4	1.6×10^7	Forced
AVA47	DU331	6.06	Delta	Counter	10	30	20	45	20	0.4	1.6×10^7	Forced
AVA48	DU331	6.06	Delta	Counter	10	30	20	55	20	0.4	1.6×10^7	Forced
AVA49	DU331	6.06	Delta	Counter	10	30	25	50	20	0.4	1.6×10^7	Forced
AVA50	DU331	6.06	Delta	Counter	10	30	20	50	25	0.4	1.6×10^7	Forced
TUD01	DU91W2250	0.6	Delta	Counter	5	17	10	35	16.4	0.2	2.0×10^6	Free
TUD02	DU91W2250	0.6	Delta	Counter	5	17	10	35	16.4	0.3	2.0×10^6	Free
TUD03	DU93W210	0.6	Delta	Counter	5	17	10	35	16.4	0.2	1.0×10^6	Free
TUD04	DU93W210	0.6	Delta	Counter	5	17	10	35	16.4	0.4	1.0×10^6	Free
TUD05	DU93W210	0.6	Delta	Counter	5	17	10	35	16.4	0.6	1.0×10^6	Free
TUD06	DU97W300	0.6	Delta	Counter	5	17	10	35	16.4	0.2	2.0×10^6	Free
TUD07	DU97W300	0.6	Delta	Counter	5	17	10	35	16.4	0.4	2.0×10^6	Free
NTU01	NTUA18	0.6	Delta	Counter	6	18	22.2	70.2	20	0.2	8.7×10^5	Forced
NTU02	NTUA18	0.6	Delta	Counter	6	18	22.2	70.2	20	0.3	8.7×10^5	Forced